

Changes in Greenland ice sheet elevation attributed primarily to snow accumulation variability

J. R. McConnell^{*}, R. J. Arthern[†], E. Mosley-Thompson[‡], C. H. Davis[§], R. C. Bales^{||}, R. Thomas[¶], J. F. Burkhart^{||} & J. D. Kyne[#]

^{*} Desert Research Institute, University & Community College System of Nevada, Reno, Nevada 89512, USA

[†] Applied Physics Laboratory, University of Washington, Seattle, Washington 98105, USA

[‡] Byrd Polar Research Centre & Department of Geography, The Ohio State University, Columbus, Ohio 43210, USA

[§] Department of Electrical Engineering, University of Missouri-Columbia, Columbia, Missouri 65211, USA

^{||} Department of Hydrology & Water Resources, University of Arizona, Tucson, Arizona 85721, USA

[¶] EG&G Services, NASA Wallops Flight Facility, Wallops Island, Virginia 23337, USA

[#] Snow & Ice Research Group, University of Nebraska, Lincoln, Nebraska 68583, USA

The response of grounded ice sheets to a changing climate critically influences possible future changes in sea level. Recent satellite surveys over southern Greenland show little overall elevation change at higher elevations, but large spatial variability^{1–3}. Using satellite studies alone, it is not possible to determine the geophysical processes responsible for the observed elevation changes and to decide if recent rates of change exceed the natural variability. Here we derive changes in ice-sheet elevation in southern Greenland, for the years 1978–88, using a physically based model of firn densification⁴ and records of annual snow accumulation reconstructed from 12 ice cores at high elevation. Our patterns of accumulation-driven elevation change agree closely with contemporaneous satellite measurements of ice-sheet elevation change, and we therefore attribute the changes observed in 1978–88 to variability in snow accumulation. Similar analyses of longer ice-core records show that in this decade the Greenland ice sheet exhibited typical variability at high elevations, well within the long-term natural variability. Our results indicate that a better understanding of ice-sheet mass changes will require long-term measurements of both surface elevation and snow accumulation.

The previously reported, 1978–88 elevation-change estimates for the southern Greenland ice sheet¹, derived from analysis of Seasat (6 July to 10 October 1978) and Geosat-Exact Repeat Mission (8 November 1986 to 7 November 1988) satellite radar altimeter data, were improved recently by adding data from the Geosat-Geodetic Mission (1 April 1985 to 30 September 1986). The updated analysis⁵ included twice as many elevation-change measurements and expanded the spatial coverage by 50%. In addition, a precise global-ocean reference network created from four years of Topex/Poseidon altimeter data was used to obtain improved corrections for altimeter radial orbit errors and measurement system biases. The updated elevation-change map includes about 90% of the area above the 2,000-m elevation contour south of 72.1° N (maximum latitude of Seasat/Geosat) and about 75% of the area west of the elevation divide between 1,700–2,000 m (Fig. 1). Effectively no coverage is available below 1,700 m because of the poor quality and limited quantity of the radar altimeter data near the ice-sheet edge⁵. The rate of elevation change (dH/dt) varies spatially from -24 to $+24$ cm yr^{-1} over distances as small as 200 km (note the strong dH/dt gradient around 66° N and the abrupt transition from positive to negative change at the elevation divide).

Between 1997 and 1999, ice cores that penetrated at least to a depth corresponding to 1978 were collected at ten locations around the southern ice sheet. All cores were analysed for a number of seasonally varying chemical species (hydrogen peroxide, calcium, ammonium, nitrate ions) using a continuous ice-core melter analysis system⁶. Two additional seasonally varying constituents, insoluble dust concentration and stable water-isotope ratios, were measured using discrete samples. In combination with field measurements of snow density, these multi-parameter glacio-chemical records were used to determine records of net annual snow accumulation at each site. Because of spatial variability in snow accumulation⁷, multiple cores were collected at four locations to identify regional-scale versus local-scale accumulation components^{8,9}. Discrete measurements of hydrogen peroxide from a core drilled in 1988 were used to develop a record of annual accumulation at Dye 3 (65.2° N, 43.9° W)¹⁰ and a 1778–1989 accumulation record was developed at Crete (71.1° N, 37.3° W) by combining published accumulation records^{11,12}.

The density of near-surface firn layers increases with depth and, in response to changing snow accumulation rates and temperature, this increase with depth also varies with time. To derive changing ice-sheet elevation from measured time series of snow accumulation, we used a model that predicts the evolution of the density–depth profile by solving coupled heat- and mass-transfer equations using a one-dimensional, lagrangian scheme, referenced to pressure coordinates⁴. The constitutive relationship for snow was calculated using rate equations for the various sintering mechanisms important in snow compaction^{13,14}. The initial depth profiles of temperature and density were obtained from steady-state calculations at the mean temperature, mean accumulation rate and mean surface density. Boundary conditions include the temperature of the ice at depth, and surface histories of temperature¹⁵, accumulation

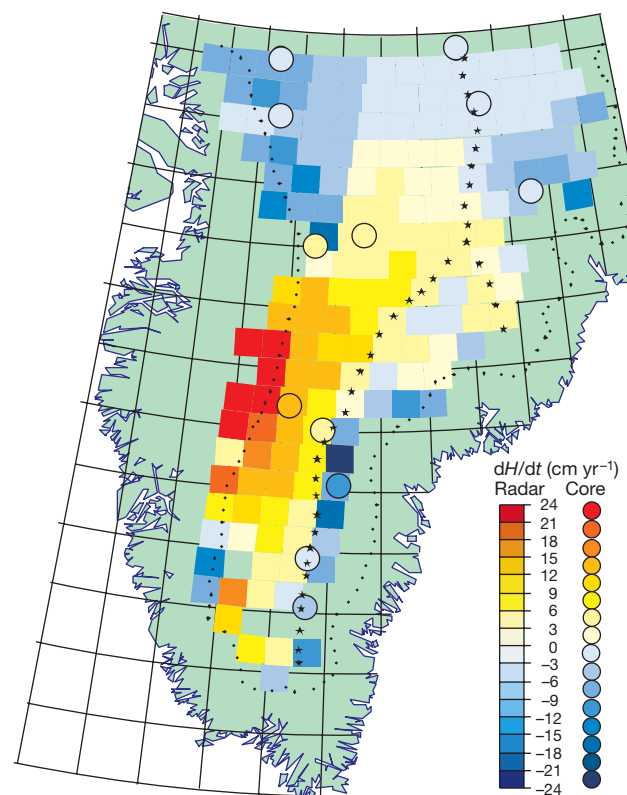


Figure 1 Accumulation-derived and radar-altimetry-derived 1978–88 ice-sheet elevation change. Shown are the approximate locations of the elevation divide (stars), the 2,000-m elevation contour (dots) and the ice-core sites (circles). The radar dH/dt values are shown in 50×50 km cells (adapted from ref. 5).

rate and density. Mean surface density was derived from the ice-core data using the zero-depth intercept of a polynomial fit to the measured density–depth profile. Densification rates for the upper two metres were also derived from the measured density profiles rather than from sintering rate equations (at shallow depths the effects of vapour transport, seasonal temperature variations and reworking by wind are important although these were not explicitly included in the sintering model). The annual temperature cycle and surface density (uppermost 1 m) in Greenland change little from year to year. Earlier calculations⁴ show that elevation changes resulting from these intra-annual variations are small compared with those resulting from inter-annual variations in snow accumulation.

The modelled change in vertical separation between the surface and the 4-MPa pressure level overburden (deep enough to lie within incompressible ice) defines the elevation change caused by variations in density⁴. The actual elevation change observed at any location is the sum of this component and the change in the local ice-equivalent-thickness (defined as the total mass of ice occupying a unit area of bedrock, divided by the density of pore-free ice). Because the divergence of the ice flow field at each core site is unknown, we cannot directly calculate the change in ice-equivalent thickness over the time period spanned by the ice core records. However, on the assumption that the ice-flow divergence is constant during this period, an estimate for the higher-frequency changes in ice-equivalent thickness can be obtained using the measured accumulation rates and added to the elevation changes predicted by the density model. We refer to the resulting time series as the ‘elevation anomaly’ at each site. These will be superimposed upon any secular trend in elevation change caused by long-term mass imbalance. Both the observed and accumulation-derived elevation changes at the twelve locations where annual accumulation data are available over the 10-year period are listed in Table 1 and shown in Fig. 1. To facilitate comparison with the radar-derived observations, 1978–88 accumulation-driven elevation change (dH/dt) is expressed in cm yr^{-1} .

We investigated the sensitivity in the calculation of accumulation-derived estimates of ice-sheet elevation change to several sources of error. To examine the sensitivity to errors in the constitutive equation for snow, strain rates in the densification model were artificially increased and decreased by a factor of ten⁴. To determine the sensitivity of our results to fluctuations in accumulation rate before the beginning of the ice-core records, we used an ensemble of six plausible ~50-year accumulation-rate histories having the same mean and inter-annual variance as the observed record in Monte-Carlo simulations. Similarly, we investigated the effects of short-scale (tens of metres) spatial variations of accumulation rate by adding noise to the measured time series and repeating these calculations for an ensemble of such records. The variance of the local noise component was obtained from closely

spaced ice cores at four of the ice-core sites^{8,9}. Note that kilometre-scale topography may also influence accumulation, although generally at multi-decadal to century, rather than annual, timescales. The 65% confidence intervals in Table 1 indicate the combined contribution from all these sources of error. Sensitivity to the accumulation history before the start of the core decreases rapidly with time under the relatively warm conditions found in Greenland⁴. Many of the core records extended to 1974 and earlier (Table 1) and for these sites, short-scale spatial variability in accumulation during the 1978–88 period provided the largest contribution to the combined uncertainties. At the six sites with shorter accumulation records, approximately half of the total uncertainty was the result of unknown accumulation before the start of the core record. If the previous accumulation were markedly different than during the core-based observation period, this would affect the results at sites with relatively short accumulation records.

The radar dH/dt values reported in Table 1 are the average of all elevation-change measurements within a circular area centred at the ice-core location. A nominal radius of 20 km was used for ten of the core locations, whereas a radius of 30 km was used at two core locations (Summit and Dye 3) where insufficient data were available within the nominal radius. Each set of data was edited by excluding elevation differences greater than two standard deviations from the primary gaussian distribution. The 65% confidence intervals include the combined contribution of random measurement error and estimates of the uncertainties in various corrections applied to the elevation data (isostatic uplift, inter-satellite bias, orbit-error corrections, and environmental corrections)^{1,5}.

Comparisons between the accumulation-derived and radar-altimeter elevation-change estimates (see Supplementary Information) indicate that the large majority of the measured change in ice-sheet elevation in southern Greenland from 1978 to 1988 is the result of temporal variability in snow accumulation. The accumulation-derived elevation change gives the same general pattern of strong thickening to the west of the elevation divide and thinning to the east. We note the excellent match in the strong radar dH/dt gradient across the ice divide from Dye 2 (66.4° N, 46.2° W) to Dye 3 (65.2° N, 43.9° W). The notable exception is in the western region along the 2,000-m contour between 69° N and 72° N where the accumulation-derived elevation change is generally smaller than the radar-based observations. A significant difference was also found in this area in a comparison between 1978–88 radar dH/dt and 1993–98 laser dH/dt results¹⁶ with no corresponding change in accumulation rate between the two time periods. Previous modelling and analysis of the Seasat and Geosat altimeter waveforms demonstrated that there was a significant temporal change in the geophysical characteristics of the near-surface snow in this particular area of the ice sheet¹⁷. Indeed, an unusually large number of melt events were found in the 69.0° N, 45.0° W core at depths corresponding to 1977 and 1978, with relatively few melt events in the early to mid-1980s. No such anomalous melt features were observed in the nearby 69.2° N, 43.0° W core where there is good

Table 1 Ice-core accumulation-derived and radar-based estimates of mean dH/dt from 1978 to 1988

Site latitude (°N), longitude (°W)	Initial year in accumulation record	1978–1988 Accumulation dH/dt (cm yr^{-1})	1978–1988 Radar* dH/dt (cm yr^{-1})
72.3, 38.0 (Summit)	1950	-1.1 (±2.9)	-0.1 (±1.5)
71.1, 37.3 (Crete)	1778	-0.7 (±4.2)	-1.9 (±1.5)
71.9, 47.5	1974	-1.9 (±2.1)	-8.0 (±1.5)
71.1, 47.2	1974	-1.1 (±2.0)	-5.1 (±2.1)
69.8, 35.0	1976	-3.8 (±1.5)	-6.2 (±1.5)
69.2, 43.0	1977	+5.8 (±1.6)	+4.5 (±1.7)
69.0, 45.0	1977	+6.9 (±2.3)	-22.3 (±1.7)
66.4, 46.2 (Dye 2)	1900	+12.7 (±2.3)	+14.9 (±1.6)
66.0, 44.5	1976	+4.8 (±1.2)	+4.7 (±1.6)
65.2, 43.9 (Dye 3)	1931	-10.3 (±2.3)	-8.6 (±1.8)
63.8, 45.0	1978	-0.4 (±2.0)	+3.7 (±1.6)
63.1, 44.8	1978	-3.2 (±2.0)	-2.3 (±1.8)

Error limits show the 65% confidence interval.

* Includes subtraction of 0.5 cm yr^{-1} uplift from long-term isostatic rebound.

Table 2 Ice core accumulation-derived estimates of the standard deviation in decadal ice-sheet elevation change (dH/dt) over the specified time ranges

Site name	Latitude (°N), longitude (°W)	Time range	Standard deviation in decadal-scale dH/dt (cm yr^{-1})
Humboldt	78.5, 56.8	1690–1994	2.4
Nasa U	73.8, 49.5	1690–1994	4.1
Summit	72.3, 38.0	1950–1998	2.0
Crete	71.1, 37.3	1778–1982	3.7
Milcent	70.3, 45.0	1177–1966	8.4
Dye2	66.4, 46.2	1900–1998	12.7
Dye3	65.2, 43.9	1931–1987	9.4

1978–88 dH/dt values for Summit, Crete, Dye 2, and Dye 3 are given in Table 1.

agreement between the radar and accumulation dH/dt estimates. These observations indicate that a large melt layer existed in 1977 and 1978 which resulted in a different radar signature at the snow–air interface than in subsequent years. This caused Geosat–Seasat dH/dt estimates to be biased towards excess thinning and/or reduced thickening in that region over the 10-year period.

To put these accumulation-derived changes in ice-sheet elevation in historical perspective, we derived estimates of dH/dt over longer time periods using previously published^{6,10,12} and new records of annual accumulation. From the annual dH/dt time series, decadal dH/dt (cm yr^{-1}) values were computed. Standard deviations in decadal dH/dt (Table 2) range from 2.0 cm yr^{-1} at the Summit location in central Greenland to 12.7 cm yr^{-1} at the southern Dye 2 site. Comparisons of the historical range of decadal dH/dt (Table 2) with the 1978–88 accumulation-derived and radar-based measurements (Table 1) indicate that recently observed changes in ice-sheet elevation above $\sim 2,000\text{-m}$ elevation are typical. Because snow accumulation at Dye 2 is highly cyclic, even the marked increase in annual accumulation from 1978 to 1988 that has led to the recent large increase in ice-sheet elevation in that region is not unusual over the last century.

These widely distributed accumulation measurements and computed elevation anomalies demonstrate that altimetry-derived estimates of ice-sheet thickening and thinning from 1978–88 over much of the southern Greenland ice sheet above $\sim 2,000\text{-m}$ elevation are consistent with elevation changes caused by temporal variability in snow accumulation. The ice-core accumulation measurements reported here do not address the significance of observed elevation change at lower elevations². Analyses of longer accumulation records indicate that the decadal-scale changes in ice-sheet elevation that occurred during 1978–88 are typical over the last few centuries and well within the natural variability of accumulation-driven elevation change. It is clear that decadal-scale variability in snow accumulation has the potential to mask longer-period changes in surface elevation associated with ice-sheet dynamics. This suggests that accurate detection of any long-term mass imbalance of the ice sheets and assessment of likely causes will require multi-decadal time series of surface elevation in conjunction with widely distributed ice-core-derived accumulation measurements collected over the time period of interest. □

Received 2 February; accepted 12 July 2000.

- Davis, C. H., Kluever, C. A. & Haines, B. J. Elevation change of the southern Greenland Ice Sheet. *Science* **279**, 2086–2088 (1998).
- Krabill, W. *et al.* Rapid thinning of parts of the southern Greenland Ice Sheet. *Science* **283**, 1522–1524 (1999).
- Zwally, H. J., Brenner, A. C. & DiMarzio, J. P. Comment: Growth of the southern Greenland Ice Sheet. *Science* **281**, 1251 (1998).
- Arthern, R. J. & Wingham, D. J. The natural fluctuations of firn densification and their effect on the geodetic determination of ice sheet mass balance. *Clim. Change* **40**, 605–624 (1998).
- Davis, C. H., Kluever, C. A., Haines, B. J., Perez, C. & Yoon, Y. T. Improved elevation change measurement of the southern Greenland Ice Sheet from satellite radar altimetry. *IEEE Trans. Geosci. Remote Sens.* **38**, 1367–1378 (2000).
- Anklin, M., Bales, R. C., Mosley-Thompson, E. & Steffen, K. Annual accumulation at two sites in northwest Greenland during recent centuries. *J. Geophys. Res.* **103**, 28775–28783 (1998).
- Van der Veen, C. J. Interpretation of short-term ice-sheet elevation change inferred from satellite altimetry. *Clim. Change* **23**, 383–405 (1993).
- McConnell, J. R., Mosley-Thompson, E., Bromwich, D. H., Bales, R. C. & Kyne, J. D. Interannual variations in snow accumulation on the Greenland Ice Sheet (1985–1996): New observations versus model predictions. *J. Geophys. Res.* **105**, 4039–4046 (2000).
- Fisher, D. A., Reeh, N. & Clausen, H. B. Stratigraphic noise in time series derived from ice cores. *Ann. Glaciol.* **7**, 76–83 (1985).
- Sigg, A. & Neftel, A. Evidence for a 50% increase in H_2O_2 over the past 200 years from a Greenland ice core. *Nature* **351**, 557–559 (1991).
- Anklin, M., Stauffer, B., Geis, K. & Wagenbach, D. Pattern of annual snow accumulation along the west Greenland flow line: no significant change observed during recent decades. *Tellus B* **46**, 294–303 (1994).
- Clausen, H. B., Gundestrup, N. S., Johnsen, S. J., Bindshadler, R. & Zwally, J. Glaciological investigations in the Crete area, central Greenland: A search for a new deep-drilling site. *Ann. Glaciol.* **10**, 10–15 (1988).
- Alley, R. B. Firn densification by grain-boundary sliding: A first model. *J. Phys. (Paris)* **48**, 249–256 (1987).
- Maeno, N. & Ebinuma, T. Pressure sintering of ice and its implication to the densification of snow at polar glaciers and ice sheets. *J. Phys. Chem.* **87**, 4103–4110 (1983).

- Ohmura, A. New temperature distribution maps for Greenland. *Z. Gletscherkunde Glazialgeol.* **23**, 1–45 (1987).
- Thomas, R. *et al.* 20-year time series of Greenland Ice-Sheet thickness change from radar and laser altimetry. *Polar Geogr.* (submitted).
- Davis, C. H. Temporal change in the extinction coefficient of snow on the Greenland ice sheet from an analysis of Seasat and Geosat altimeter data. *IEEE Trans. Geosci. Remote Sens.* **34**, 1066–1073 (1996).

Supplementary information is available on Nature's World-Wide Web site (<http://www.nature.com>) or as paper copy from the London editorial office of Nature.

Acknowledgements

We acknowledge D. Belle-Oudry, M. Hutterli, B. Snider, E. Kline, Z. Li, P.-N. Lin, V. Zagorodnov, E. Ramsey, the Twin Otter and LC-130 aircraft crews and others for assistance in the laboratory and the field. This work was supported by grants from NASA and the US NSF.

Correspondence and requests for materials should be addressed to J.M. (email: jmconn@dri.edu).

Evidence for iron, copper and zinc complexation as multinuclear sulphide clusters in oxic rivers

Tim F. Rozan*, Michael E. Lassman†, Douglas P. Ridge† & George W. Luther III*

*College of Marine Studies, University of Delaware, 700 Pilottown Road, Lewes, Delaware 19958, USA

†Department of Chemistry and Biochemistry, Lamont duPont Laboratory, University of Delaware, Newark, Delaware 19716, USA

The availability and toxicity of trace metals in fresh water are known to be regulated by the complexation of free metal ions with dissolved organic matter^{1–3}. The potential role of inorganic sulphides in binding trace metals has been largely ignored because of the reduced persistence of sulphides in these oxic waters. However, nanomolar concentrations of copper and zinc sulphides have been observed in four rivers in Connecticut and Maryland^{4,5}. Here we report dissolved ($< 0.2 \mu\text{m}$ particle diameter) sulphide concentrations ranging up to 600 nM, with more than 90% being complexed by copper, iron and zinc. These complexes account for up to 20% of the total dissolved Fe and Zn and 45% of the total dissolved Cu. Fourier transform mass spectrometry reveals that these complexes are not simple $\text{M}(\text{HS})^+$ protonated species^{6,7} but are higher-order unprotonated clusters (M_3S_3 , M_4S_6 , M_2S_4), similar to those found in laboratory solutions^{8–10} and bio-inorganic molecules¹¹. These extended structures have high stability constants^{8,10} and are resistant to oxidation and dissociation^{10,12}, which may help control the toxicity of these and other less abundant, but more toxic, trace metals, such as silver, cadmium and mercury.

We found the total dissolved sulphide (DS_T) concentrations and metal sulphide speciation in river waters to be strongly correlated with the extent of watershed development. DS_T , defined as Σ Fe sulphides + Cu sulphides + Zn sulphides + other soft class B metal sulphides (Ag , Cd , Hg , Pb) + $\text{HS}^- + \text{S}_x^{2-} + \text{S}^0$, was found in concentrations ranging between 20 and 580 nM (Table 1). High DS_T ($> 200 \text{ nM}$) was found in rivers that drained urbanized areas that received inputs of treated sewage effluent. In these rivers, the metal sulphide speciation, as determined by electrochemical analysis^{4,5,13,14}, consisted of metal sulphide complexes in the following order of concentration abundance: Fe sulphides ($\Sigma \text{FeS} + \text{FeSH}^+$) \gg Zn sulphides $>$ Cu sulphides $>$ (polysulphides). Polysulphides ($\text{S}_{4,5}^{2-}$), which are partly oxidized sulphide species that are reduced by $\text{Cr}(\text{II})$, were only electrochemically measured¹⁵ in low

is less than 100%). Models for the additional oligonucleotide, GTP molecules and Mg^{2+} ions, have been fitted into electron density maps and refinement of these oligo- Mn^{2+} -polymerase and oligo-GTP-Mg-Mn-polymerase complexes against their data sets, imposing strict threefold NCS constraints, resulted in models with *R* factors of 23.7 and 21.4%, respectively, and good stereochemistry (Table 1).

Figures

Unless otherwise stated figures were drawn using BOBSCRIPT²⁶ and rendered with RASTER3D²⁷.

Received 2 August; accepted 28 December 2000.

1. Reinisch, K. M., Nibert, M. L. & Harrison, S. C. Structure of the reovirus core at 3.6 Å resolution. *Nature* **404**, 960–967 (2000).
2. Grimes, J. M. *et al.* The atomic structure of the bluetongue virus core. *Nature* **395**, 470–478 (1998).
3. Makeyev, E. V. & Bamford, D. H. Replicase activity of purified recombinant protein P2 of double-stranded RNA bacteriophage φ6. *EMBO J.* **19**, 124–133 (2000).
4. Butcher, S. J., Makeyev, E. V., Grimes, J. M., Stuart, D. I. & Bamford, D. H. Crystallization and preliminary X-ray crystallographic studies on the bacteriophage φ6 RNA-dependent RNA polymerase. *Acta Crystallogr. D* **56**, 1473–1475 (2000).
5. Mindich, L. Reverse genetics of dsRNA bacteriophage φ6. *Adv. Virus Res.* **53**, 341–353 (1999).
6. Gottlieb, P., Strassman, J., Quao, X., Frucht, A. & Mindich, L. In vitro replication, packaging, and transcription of the segmented, double-stranded RNA genome of bacteriophage φ6: studies with procapsids assembled from plasmid-encoded proteins. *J. Bacteriol.* **172**, 5774–5782 (1990).
7. Mindich, L. Precise packaging of the three genomic segments of the double-stranded-RNA bacteriophage φ6. *Microbiol. Mol. Biol. Rev.* **63**, 149–160 (1999).
8. Makeyev, E. V. & Bamford, D. H. The polymerase subunit of a dsRNA virus plays a central role in the regulation of viral RNA metabolism. *EMBO J.* **19**, 124–133 (2000).
9. Ollis, D. L., Kline, C. & Steitz, T. A. Domain of *E. coli* DNA polymerase I showing sequence homology to T7 DNA polymerase. *Nature* **313**, 818–819 (1985).
10. Delarue, M., Poch, O., Tordo, N., Moras, D. & Argos, P. An attempt to unify the structure of polymerases. *Protein Eng.* **3**, 461–467 (1990).
11. Lesburg, C. A. *et al.* Crystal structure of the RNA-dependent RNA polymerase from hepatitis C virus reveals a fully encircled active site. *Nature Struct. Biol.* **6**, 937–943 (1999).
12. Ago, H. *et al.* Crystal structure of the RNA-dependent RNA polymerase of hepatitis C virus. *Struct. Fold. Des.* **7**, 1417–1426 (1999).
13. Bressanelli, S. *et al.* Crystal structure of the RNA-dependent RNA polymerase of hepatitis C virus. *Proc. Natl Acad. Sci. USA* **96**, 13034–13039 (1999).
14. Stuart, D. I., Levine, M., Muirhead, H. & Stammers, D. K. Crystal structure of cat muscle pyruvate kinase at resolution of 2.6 Å. *J. Mol. Biol.* **134**, 109–142 (1979).
15. Oh, J. W., Ito, T. & Lai, M. M. A recombinant hepatitis C virus RNA-dependent RNA polymerase capable of copying the full-length viral RNA. *J. Virol.* **73**, 7694–7702 (1999).
16. Lohmann, V., Overton, H. & Bartenschlager, R. Selective stimulation of hepatitis C virus and pestivirus NS5B RNA polymerase activity by GTP. *J. Biol. Chem.* **274**, 10807–10815 (1999).
17. Frilander, M., Poranen, M. & Bamford, D. H. The large genome segment of dsRNA bacteriophage φ6 is the key regulator in the in vitro minus and plus strand synthesis. *RNA* **1**, 510–518 (1995).
18. van Dijk, A. A., Frilander, M. & Bamford, D. H. Differentiation between minus- and plus-strand synthesis: polymerase activity of dsRNA bacteriophage φ6 in an in vitro packaging and replication system. *Virology* **211**, 320–323 (1995).
19. Huang, H., Chopra, R., Verdine, G. L. & Harrison, S. C. Structure of a covalently trapped catalytic complex of HIV-1 reverse transcriptase: implications for drug resistance. *Science* **282**, 1669–1675 (1998).
20. Zhong, W., Uss, A. S., Ferrari, E., Lau, J. Y. & Hong, Z. De novo initiation of RNA synthesis by hepatitis C virus nonstructural protein 5B polymerase. *J. Virol.* **74**, 2017–2022 (2000).
21. Yazaki, K. & Miura, K. Relation of the structure of cytoplasmic polyhedrosis virus and the synthesis of its messenger RNA. *Virology* **105**, 467–479 (1980).
22. Hendrickson, W. A. Determination of macromolecular structures from anomalous diffraction of synchrotron radiation. *Science* **254**, 51–58 (1991).
23. Brunger, A. T. *et al.* Crystallography and NMR system: A new software suite for macromolecular structure determination. *Acta Crystallogr. D* **54**, 905–921 (1998).
24. Navaza, J. AMoRe: an automated package for molecular replacement. *Acta Crystallogr. A* **50**, 164–182 (1994).
25. Laskowski, R. A., MacArthur, M. W., Moss, D. S. & Thornton, J. M. PROCHECK: a program to check the stereochemical quality of protein structures. *J. Appl. Crystallogr.* **26**, 283–291 (1993).
26. Esnouf, R. M. An extensively modified version of MolScript that includes greatly enhanced colouring capabilities. *J. Mol. Graph.* **15**, 132–134 (1997).
27. Merritt, E. A. & Bacon, D. J. in *Macromolecular Crystallography* (eds Carter, J. W. Jr & Sweet, R. M.) 505–524 (Academic, San Diego, 1997).
28. Nicholls, A., Sharp, K. A. & Honig, B. Protein folding and association: insights from the interfacial and thermodynamic properties of hydrocarbons. *Proteins* **11**, 281–296 (1991).

Supplementary information is available on Nature's World-Wide Web site (<http://www.nature.com>) or as paper copy from the London editorial office of Nature.

Acknowledgements

J. Diprose and G. Sutton helped with synchrotron data collection; J. Diprose and S. Ikemizu with calculations; and R. Esnouf and K. Harlos with computing and in-house data collection. We thank the staff at the beamlines of the ESRF, SRS and APS, in particular Sergey Korolev at the APS for help with the MAD experiment. S.J.B. is a Marie Curie Fellow. J.M.G. is funded by the Royal Society and D.I.S. by the Medical Research Council. The work was supported by the Academy of Finland, the Medical Research Council and the European Union.

Correspondence and requests for materials should be addressed to D.I.S. (e-mail: dave@strubi.ox.ac.uk). Coordinates have been deposited in the RCSB Protein database under accession codes: 1HHS, 1HHT, 1HI0, 1HI1, 1HI8.

correction

Improved estimates of global ocean circulation, heat transport and mixing from hydrographic data

Alexandra Ganachaud & Carl Wunsch

Nature **408**, 453–457 (2000).

In this first paragraph of this paper, the uncertainty on the net deep-water production rates in the North Atlantic Ocean was given incorrectly. The correct value should have been $(15 \pm 2) \times 10^6 \text{ m}^3 \text{ s}^{-1}$. □

errata

Changes in Greenland ice sheet elevation attributed primarily to snow accumulation variability

J. R. McConnell, R. J. Arthern, E. Mosley-Thompson, C. H. Davis, R. C. Bales, R. Thomas, J. F. Burkhard & J. D. Kyne

Nature **406**, 877–879 (2000).

As the result of an editing error, the 1993–1998 aircraft-based altimetry surveys of the southern Greenland ice sheet reported by Krabill *et al.* (1999) were erroneously described as satellite-based. □

Genome sequence of enterohaemorrhagic *Escherichia coli* O157:H7

Nicole T. Perna, Guy Plunkett III, Valerie Burland, Bob Mau, Jeremy D. Glasner, Debra J. Rose, George F. Mayhew, Peter S. Evans, Jason Gregor, Heather A. Kirkpatrick, György Pósfai, Jeremiah Hackett, Sara Klink, Adam Boutin, Ying Shao, Leslie Miller, Erik J. Grotbeck, N. Wayne Davis, Alex Lim, Eileen T. Dimalanta, Konstantinos D. Potamouisis, Jennifer Apodaca, Thomas S. Anantharaman, Jieyi Lin, Galex Yen, David C. Schwartz, Rodney A. Welch & Frederick R. Blattner

Nature **409**, 529–533 (2001).

The Genbank accession number for the annotated sequence given in this paper was typeset incorrectly. The correct accession number is AE005174. □